Eng. Sci., 2021, **15**, 95–104

Engineered Science

DOI: https://dx.doi.org/10.30919/es8d448

Maxwell-Wagner Relaxation in Ca-, Sm- and Nd-doped Ceria

Rida Ahmed,[1] Shuting Wang,[2] Sajid ur Rehman,[3] Jie Sun,[4] Jin Wang,[2] Renjun Si,[2] Ankang Zhu,[5] Yi Yu,[2] Qiuju Li[2] and Chunchang Wang[2, 6,*]

Abstract

Doped ceria, *i.e*. $Ce_{1-x}M_xO_{2-\delta}$ with M being dopant metal, has been a focus of great attention for solid oxide fuel cells (SOFCs) due to their high oxygen conduction. In the past literature, the dielectric relaxations in these materials have been ascribed to be caused by defect associates (MCe″-V*ö*) possessing different MCe″ and V*ö* distances. But we believe that with changing measurement and analysis techniques, it is necessary to invest our time to re-examine the already reported materials and take a detailed investigation of the underlying phenomenon behind their dielectric relaxations again. Thus, we have used solid-state reaction to prepare $Ce_{1-x}M_xO_{2-\delta}$ with M=Ca, Sm, and Nd in x=0.1, 0.2, and 0.3 ratios, respectively. The as-prepared and post annealed samples were tested for dielectric properties from 300-1080 K with varying frequencies. The low-temperature relaxation (R1) was argued to be a Maxwell-Wagner relaxation caused by humidity sensitivity. The high-temperature relaxation (R2) was ascribed to be caused by the hopping motion of oxygen vacancies. This fact was also supported by a detailed analysis of impedance spectra. While according to the previous reports, this relaxation is because of the oxygen-vacancy-dopant defect pair.

Keywords: Dielectric; Maxwell-Wagner relaxations; Defects; Impedance.
Received: 12 January 2021; Accepted date: 30 March 2021.
Article type: Research article.

1. Introduction

Ionic conducting oxides, especially ceria and its compounds, have acquired fame for the manufacture of solid oxide fuel cells, oxygen sensors and electrochemical applications.[1–4] Different dopants have been added to the ceria matrix according to the required applications in the past literature. The properties of ceria vary remarkably with different dopants and their concentrations. Although extensive literature can be found on the effect of the desired dielectric properties with specific dopants in ceria, most of the work select the dopant to be 1) either a single element 2) or multiple elements belonging to the same group (hence same valence state and properties) of the periodic table.[5-6] Also, among it, about every other work is on the Lanthanides series.[6] This conventional selection of dopants gives rise to the questions in the mind of the reader: are lanthanides the only suitable elements for ceria doping? Will the dielectric permittivity change with the change of dopants? Would the nature of the dielectric relaxations alter with the change of dopant?

In the present work, we have selected one alkaline earth element (Ca) and two 3d transition elements (Sm and Nd) as dopants so a clear understanding can be made about the nature of the dielectric relaxations. Ceria (CeO_2) is a fluorite-structured compound showing ionic (oxygen) conduction. The Ce ion exists in a tetravalent state and when is doped with lesser valent ions, such as di-valent (M^{2+}) and tri-valent (M^{3+}) dopants, charge imbalance is created in the fluorite structure, which is compensated with the generation of oxygen vacancies (V_O).[5] These vacancies become mobile with the elevation of temperature making ceria a good oxygen-ion conducting electrolyte. Because of this factor, it has one of the major applications as an electrolyte in solid oxide fuel cells.[6] A single divalent dopant ion produces one oxygen vacancy, whereas it takes two trivalent dopants to generate a single vacancy.[7–12] In the past work, it has been reported that mostly the dopant ions and oxygen vacancies associate to form MV_O

[1] *Institute of Solid State Physics, Chinese Academy of Sciences, Hefei 230031, PR China.*
[2] *Laboratory of Dielectric Functional Materials, School of Physics & Material Science, Anhui University, Hefei, 230601, P. R. China.*
[3] *High Magnetic Field Laboratory, Chinese Academy of Sciences, Hefei 230031, Anhui, P. R. China.*
[4] *State Key Laboratory of ASIC & System, School of Microelectronics, Fudan University, Shanghai 200433, China.*
[5] *Institutes of Physical Science and Information Technology, Anhui University, Hefei 230601, P. R. China*
[6] *State Key Laboratory of Low-Dimensional Quantum Physics, Department of Physics, Tsinghua University, Beijing 100084, P. R. China.*
* *Email:* ccwang@ahu.edu.cn (C. Wang)

pairs and isolated M ion carrying an effective positive and negative charge respectively and rarely associate to generate neutral M_2V_O triplet.[13,14] According to Kroger-Vink notation:

$$M_2O_3 \rightarrow (M_{Ce}V_o)^{\cdot} + M'_{Ce} + 3O^{x}_{O} \quad (1)$$

These MV_O pairs are considered to be responsible for creating dielectric dipoles that give rise to Debye relaxations in the doped ceria.[15,16]

There are reports where the dielectric behaviour and relaxations for pure ceria are the same as those of doped one.[17] It means that MV_O pairs cannot be the only reason for this anticipation stimulated us to perform a detailed dielectric study on doped ceria to verify the origin of relaxation peaks. Ca, Sm and Nd have been used as dopants for ceria, and their dielectric behaviour has been analyzed.[17] Dopants ratio in ceria have been varied, and a comparison is made to which percentage of an element gives the highest value of dielectric response. Yamamura *et al*. have prepared $Ce_{1-x}Ca_xO_{2-\delta}$, $Ce_{1-x}Sm_xO_{2-\delta}$ and $Ce_{1-x}Nd_xO_{2-\delta}$ with ratios varying from 0.1 to 0.9 and have studied their dielectric properties.[18–20] where the values of 0.1, 0.2 and 0.3 gave the highest permittivity values for Ca, Sm and Nd, respectively. However, they have ascribed both of the relaxations to be caused by defect associates (MCe''-$V\ddot{o}$) possessing different MCe'' and $V\ddot{o}$ distances. Whereas, we believe that the high-temperature relaxation maybe a Maxwell-Wagner relaxation. Thus, in this works we have prepared $Ce_{0.9}Ca_{0.1}O_{2-\delta}$, $Ce_{0.8}Sm_{0.2}O_{2-\delta}$ and $Ce_{0.7}Nd_{0.3}O_{2-\delta}$ by solid-state reaction and a detailed analysis of the dielectric properties of the as-prepared and oxygen annealed samples has been performed in order to analyze the true nature of the relaxations.

2. Experimental section

2.1 Synthesis Procedure

CeO_2 (99.9% Aldrich co.) was taken as the starting material. $CaCO_3$ (99.9% Aldrich co.) Sm_2O_3 (99.9% Aldrich co.) and Nd_2O_3 (99.9% Aldrich co.) were doped in 10 wt.%, 20 wt.% and 30% with respect to ceria. The powders were mortared for about 60 minutes by hand until they were completely mixed. The powders were then calcined at 800 ℃ for 2 h and 1000 ℃ for 5 h. Ca was completely doped in ceria while Sm and Nd didn't react completely with ceria and hence were again heated for 10 h at 1500 ℃. Single phased $Ce_{0.9}Ca_{0.1}O_{2-\delta}$ (CCO), $Ce_{0.8}Sm_{0.2}O_{2-\delta}$ (CSO) and $Ce_{0.7}Nd_{0.3}O_{2-\delta}$ (CNO) were prepared as can be evidenced by X-ray diffraction (XRD) analysis.

Rectangular pellets of uniform thickness (1.5 mm) were made for CCO, CSO and CNO with the addition of PVA. The pellets were first sintered at 600 ℃ for 2 h to ensure the complete removal of PVA and then were sintered at 1600 ℃ for 10 h.

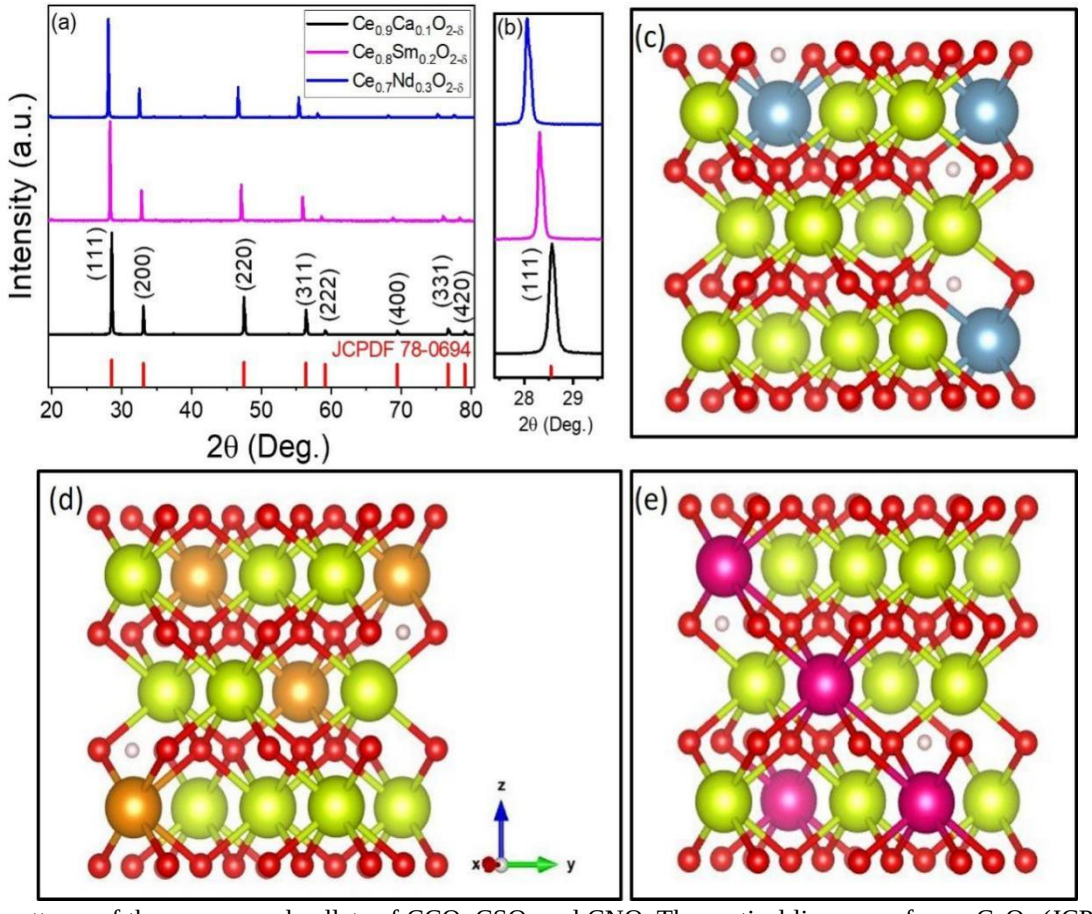

Fig. 1 (a) XRD patterns of the as-prepared pellets of CCO, CSO, and CNO. The vertical lines are of pure CeO_2 (JCPDF 78-0694). (b) The focused (111) peak showing a shift in 2θ with dopant concentration. Ball-and-stick representations of the cubic fluorite structure of (c) CCO, (d) CSO and, (e) CNO.

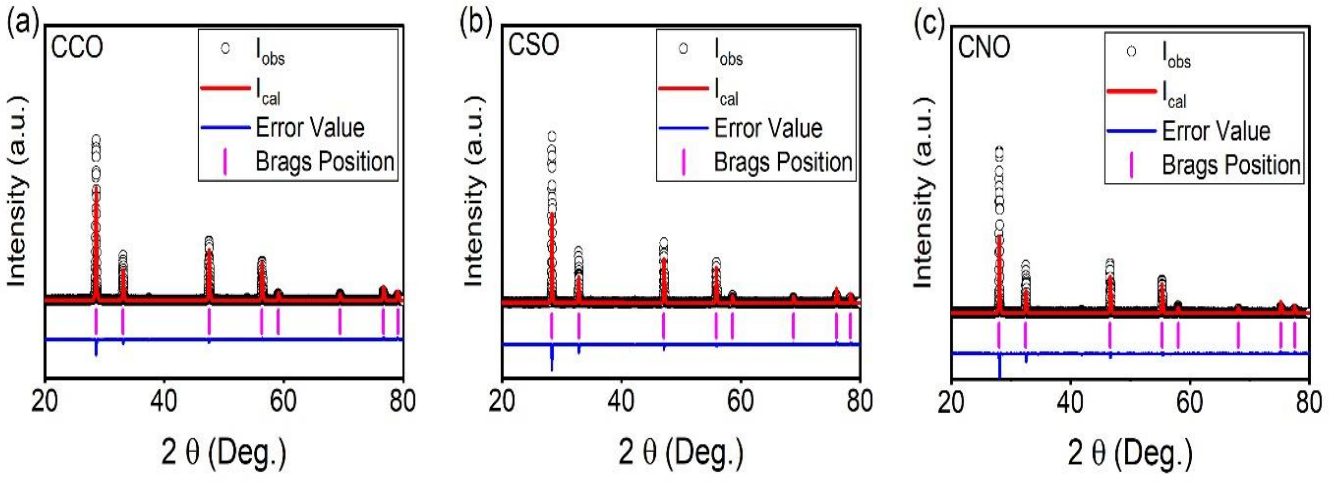

Fig. 2 The Rietveld refinement XRD patterns of (a) CCO, (b) CSO and (c) CNO.

2.2 Characterization

XRD analysis was performed by Smart Lab diffractometer (Rigaku Smartlab Beijing Co, Beijing, China) with Cu Kα radiation. A field emission scanning electron microscope (SEM, Model S-4800, Hitachi Co., Tokyo, Japan) was used to study the morphology of the pellet surfaces. Dielectric measurements and impedance analysis were performed in high temperature range from room temperature to 800 ℃ by a Wayne Kerr 6500B precise impedance analyser (Wayne Kerr Electronic Instrument Co., Shenzhen, China).

3. Results and discussions

Fig. 1(a) shows the XRD patterns of the CCO, CSO, and CNO with reference to the pure ceria peaks (JCPDF 78-0694). We can see that with the increase of dopants ratios, the peak positions have shifted towards the left side of the reference line (Fig. 1(b)). The continuous shift in the peaks with the change of dopant concentration (Ca=10%, Sm=20%, and Nd=30%) shows that the increase in dopant concentration causes distortion in the lattice structure. Also, no impurity peaks are observed, indicating that all the samples are single phase. The Rietveld refinement XRD of the samples is shown in Fig. 2. By careful examination, the peaks matched perfectly with Bragg's position peaks (shown in pink) with error values (shown in blue), indicating that no impure phase of ceria exists in any of the samples. The details of the XRD parameters, an average of crystallite size and lattice constant are calculated by as shown in Table 1. It can be seen that lattice constant is continuously increasing with the change of dopants. This is because of the distortions created by doping of heavier atoms in place of Ce ions in the matrix. Ceria, having a cubic fluorite

Table 1. XRD characterization data of CCO, CSO and CNO.

Parameters	CCO	CSO	CNO
Crystal system	cubic	cubic	cubic
Space group	Fm-3m	Fm-3m	Fm-3m
Lattice constant	A=5.413Å	a=5.433Å	a=5.463Å
Crystallite Size	55.4nm	67.45	69.71

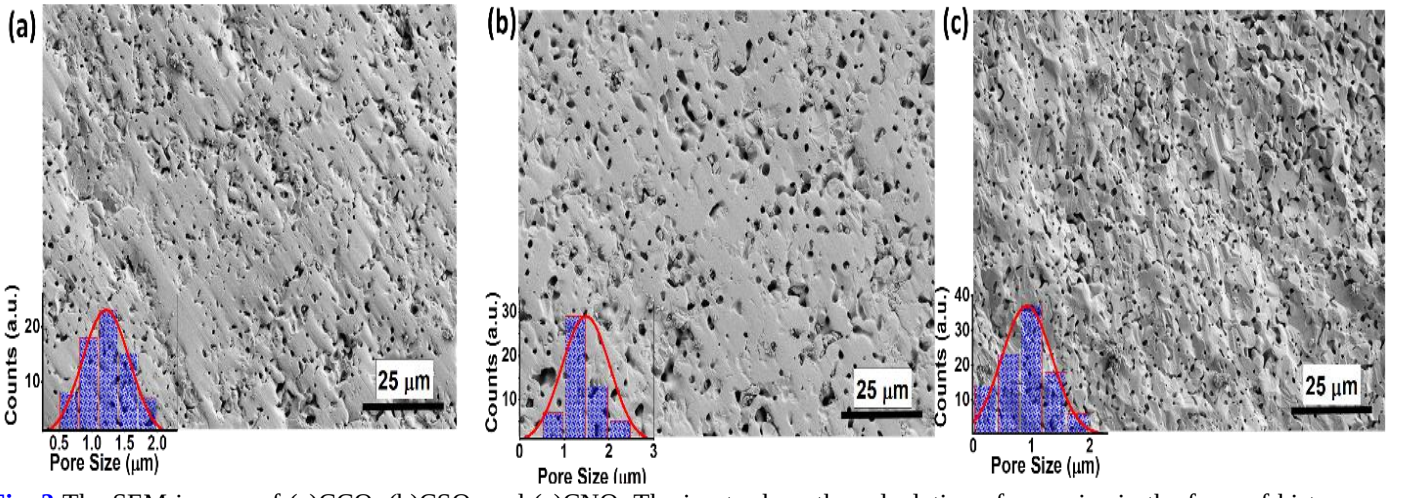

Fig. 3 The SEM images of (a)CCO, (b)CSO, and (c)CNO. The insets show the calculation of pore size in the form of histograms through standard deviation for each sample.

structure, belongs to $Fm\bar{3}m$ space group. This implies that it has four CeO_2 formula unit per cell. The unit cells have high symmetry with lattice parameter a=5.411 Å. The Ce and O atoms occupy (0,0,0) and (1/4, 1/4, 1/4) atomic sites. In an undoped ceria structure, a single Ce atom is surrounded by eight O atoms on the cubes' edges. Thus, when dopant atoms are introduced into the lattice matrix, oxygen vacancies will be generated.[21] Fig. 1(c-e) shows the lattice structures (created by VESTA-JP-Minerals) of Ca, Sm and Nd doped ceria with oxygen vacancies generated as a result of dopant atoms.

Fig. 3 shows the SEM images of the as-prepared pellets. The images show the polished and thermally etched cross-section of the pellets. The pore size is calculated through standard deviation by SEM images and shown in histograms in insets. The average pore size is almost the same for all three samples, as shown in the insets of Fig. 3. However, we can see that the average pore count is maximum for CNO and least for CCO. The generation of pores is justifiable as the replacement of Ce^{3+} ions (ionic radius~0.97Å) with dopants of higher ionic radii (Ca ~1.12Å, Sm~1.079Å and Nd~1.109Å) generates tensile stress in the samples. To reduce the stress, it is energetically favourable for the samples to create pores throughout the grains.[17]

XPS analysis of the as-prepared CCO, CSO and CNO samples were shown in Fig. 4. Ce exists in two valency states of +4 and +3 and their concentration is almost same for all the samples as shown in Fig. 4(a). The spectra of O ions of CCO, CSO and CNO samples has been deconvoluted into three Gaussian peaks in Fig. 4(b) locating at 528.9, 530.8, and 531.9 eV corresponding to lattice oxygen (LO), oxygen vacancy (VO), and chemically absorbed H_2O (CO), respectively.[22–31] The doping of Ca, Sm, and Nd has created many oxygen vacancies as can be seen from the XPS spectra. The O spectra also show that CO peak due to adsorbed water is also present in all three samples, meaning that it can be used for humidity sensitivity measurements. The XPS spectra of Ca, Sm and Nd is also shown in Fig. 4(c-e) shows that Ca exists in a single ionic state in CCO whereas Sm and Nd are divalent in CSO and CNO, respectively.

The temperature dependence of dielectric constant (ε′) of as-prepared samples of CCO, CSO and CNO were shown in Fig. 5, respectively. The dielectric constant shows step-wise relaxations beyond 400 K for all three samples. Corresponding relaxation peaks are also observed in the tanδ curves in the insets of Fig. 5. Another set of relaxation is observed at a

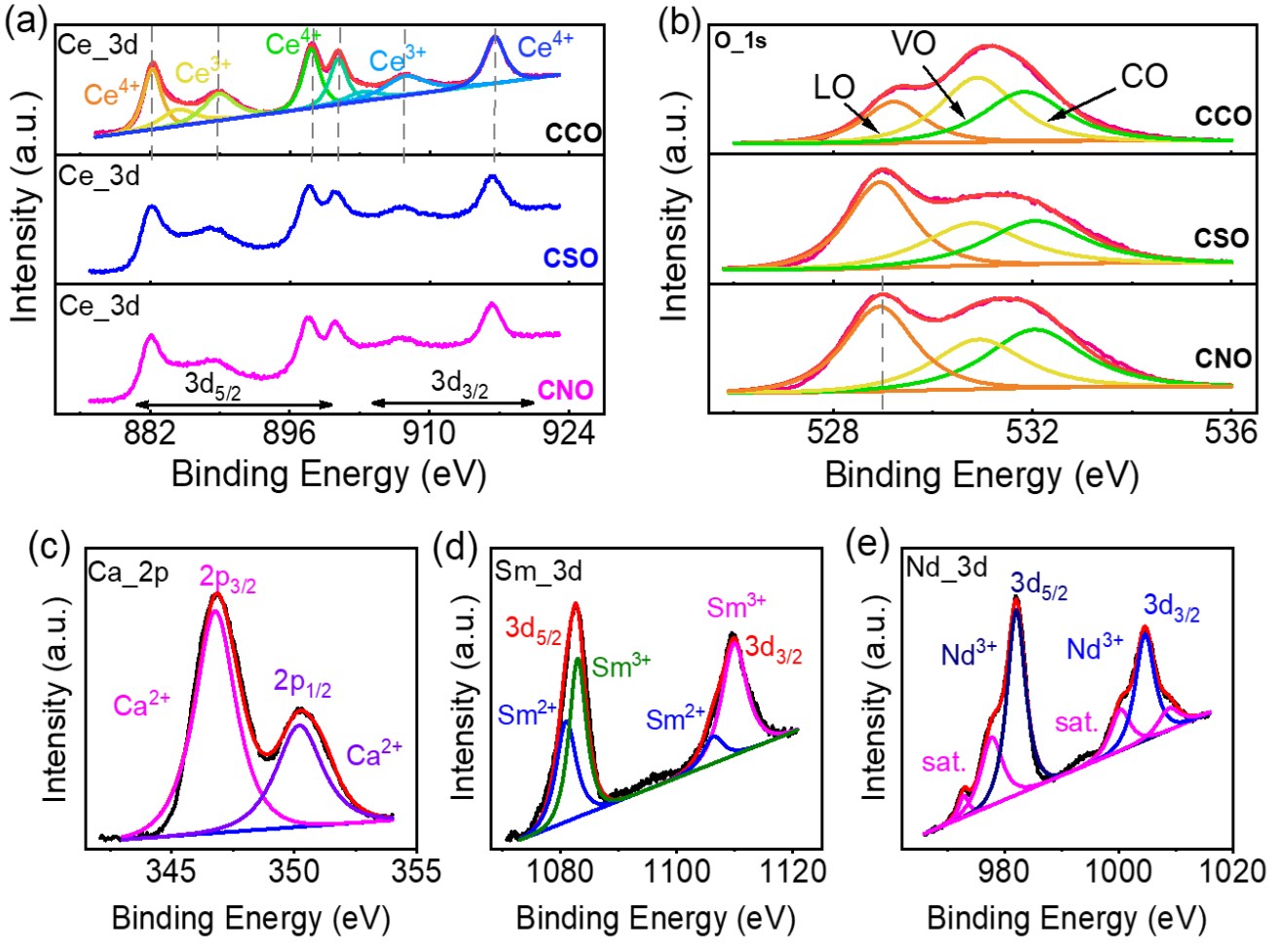

Fig. 4 The XPS images of (a) Ce ions and (b) O ions of the as-prepared samples. Ca ion concentration in CCO(c), Sm ion concentration in CSO(d), and Nd ion concentration in CNO(e).

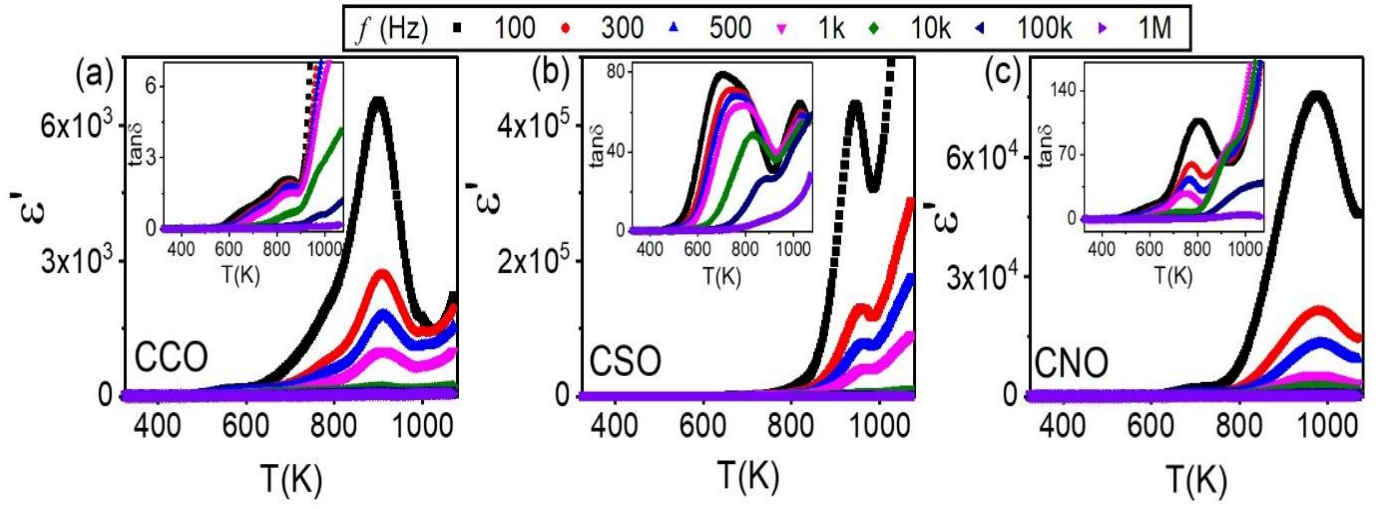

Fig. 5 Temperature dependent permittivity and tangent loss (inset) for as-prepared (a) CCO, (b) CSO, and (c) CNO recorded with different frequencies.

higher temperature, whose peak position changes with the increase in frequencies. A noticeable shift in peak positions is seen towards higher temperature for all three samples with the increase in frequency. This shows that the relaxations are thermally activated. Relaxation time (τ) plays a vital role in thermally activated relaxations as it dominates their peak positions. Peaks in the curves are obtained at a specific frequency when ωτ = 1 and then begins to decrease with the increase in temperature. The relaxations in all the samples seem shadowed. To remove the background's shadowing, the imaginary part of the electric modulus M″(T) is usually calculated as a function of temperature and plotted to reveal the relaxation phenomenon.

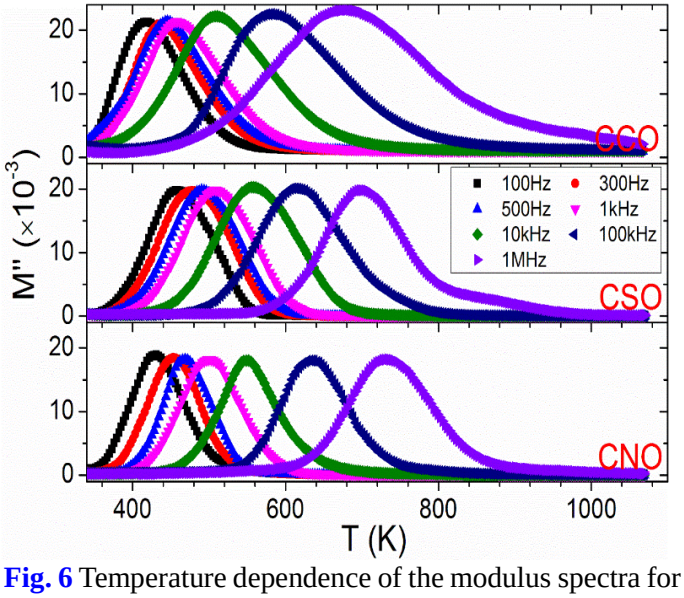

Fig. 6 Temperature dependence of the modulus spectra for CCO, CSO, and CNO recorded with different frequencies.

The temperature-dependent dielectric properties of the as-prepared CCO, CSO, and CNO samples were investigated in terms of electric modulus spectra and summarized in Fig. 6. The electric modulus spectra were used because the oxygen-ion conducting electrolytes frequently exhibit notable conductivity, especially in the temperature higher than room temperature. This conductivity can yield remarkable increasing background that shadows the dielectric relaxation. In this case, the electric modulus, defined as $M* = M' + jM'' = 1/\varepsilon*$ ($M'$and $M''$are the real and imaginary parts of $M*, j = \sqrt{-1}$), can effectively eliminate the background.[19]

At first glance, Fig. 6 shows one set of thermally activated relaxation peaks for all samples. However, a careful examination reveals that the peaks are composed of two close relaxation processes. To shed light on these relaxations, the curves were fitted using two Gaussian peaks to detach the peaks. As an example, the fitting results of CCO were displayed in Fig. 7, and the fitting results of CSO and CNO were given in Fig. S1 and S2. Perfect agreement between the experimental data (points) and the fitting results (solid curves) are achieved, indicating that the samples possess two thermally activation relaxation processes.[32] For brevity, the low-and high-temperature relaxations are named as R_1 and R_2, respectively.

Table 2. Relaxation parameters for CCO, CSO, and CNO.

Sample	R1		R2	
	E_a (eV)	f_0 (Hz)	E_a (eV)	f_0 (Hz)
CCO	0.83	2.40×10^{12}	1.05/0.60	8.47×10^{13}/4.57 $\times10^{9}$
CSO	1.02	2.09×10^{13}	0.99	1.11×10^{12}
CNO	0.83	3.98×10^{11}	0.96	1.69×10^{12}

Based on the fitting results, the peak positions can be accurately deduced. The measurement frequency (f) was plotted as a function of the peak position (T_P), according to the Arrhenius law:

$$f = f_0\, exp(-E_a/k_BT) \quad (2)$$

where f_0 is the pre-exponential factor, $E_a$is the activation

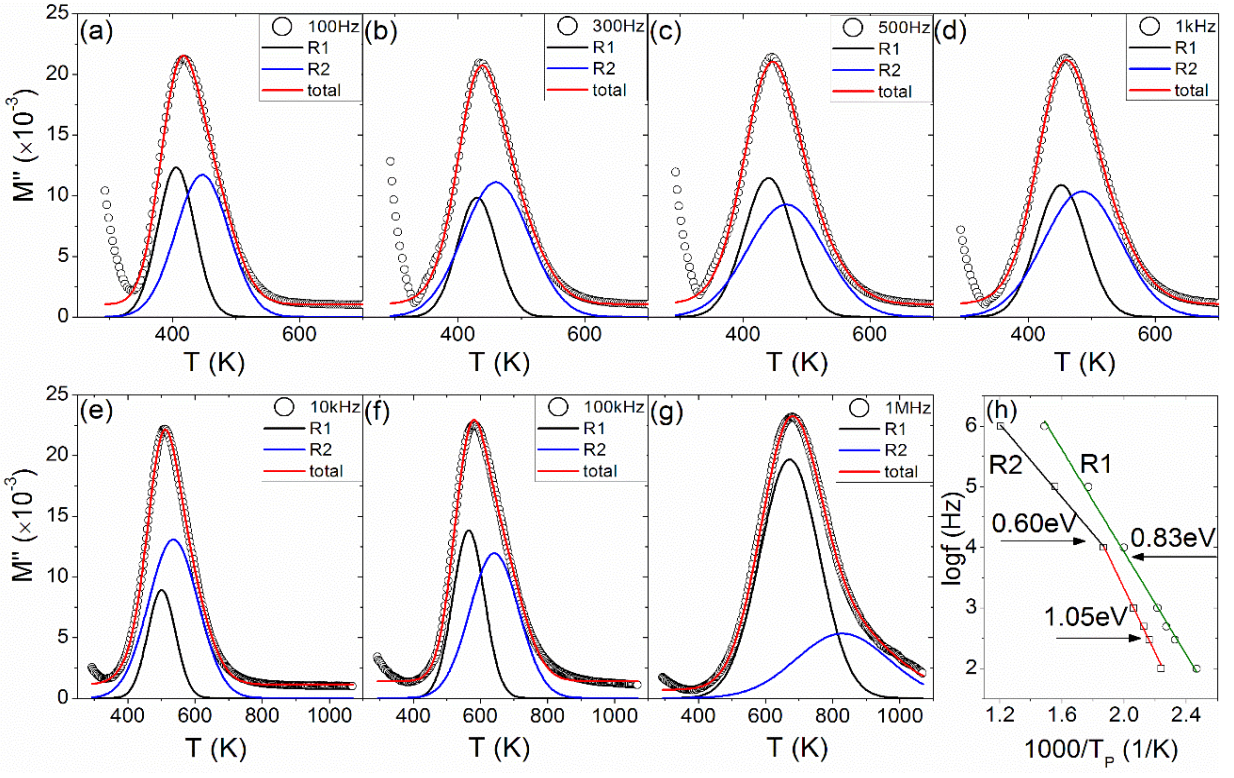

Fig. 7 Two-relaxation fittings for the electric modulus spectra of CCO (a-g) and the resultant Arrhenius plots of the relaxations (h).

energy, and k_B is the Boltzmann constant. The relaxation parameters of $f_0$and $E_a$were calculated by linear fittings and the values for all the three samples were given in Table 2.

From which one notes that the activation energy for R1 and R2 lies between 0.6-1.2 eV. This binding energy is for the dielectric relaxation caused by thermally activated oxygen vacancies migration.[20-24] Besides, the Arrhenius plot of CCO exhibits two-segment nature. The low-Tsegment shows an activation energy of 1.05 eV, whereas the high-Tone shows much lower activation energy of 0.60 eV. This feature is a hallmark of oxygen vacancies transforming from hopping conduction to band conduction.[20]

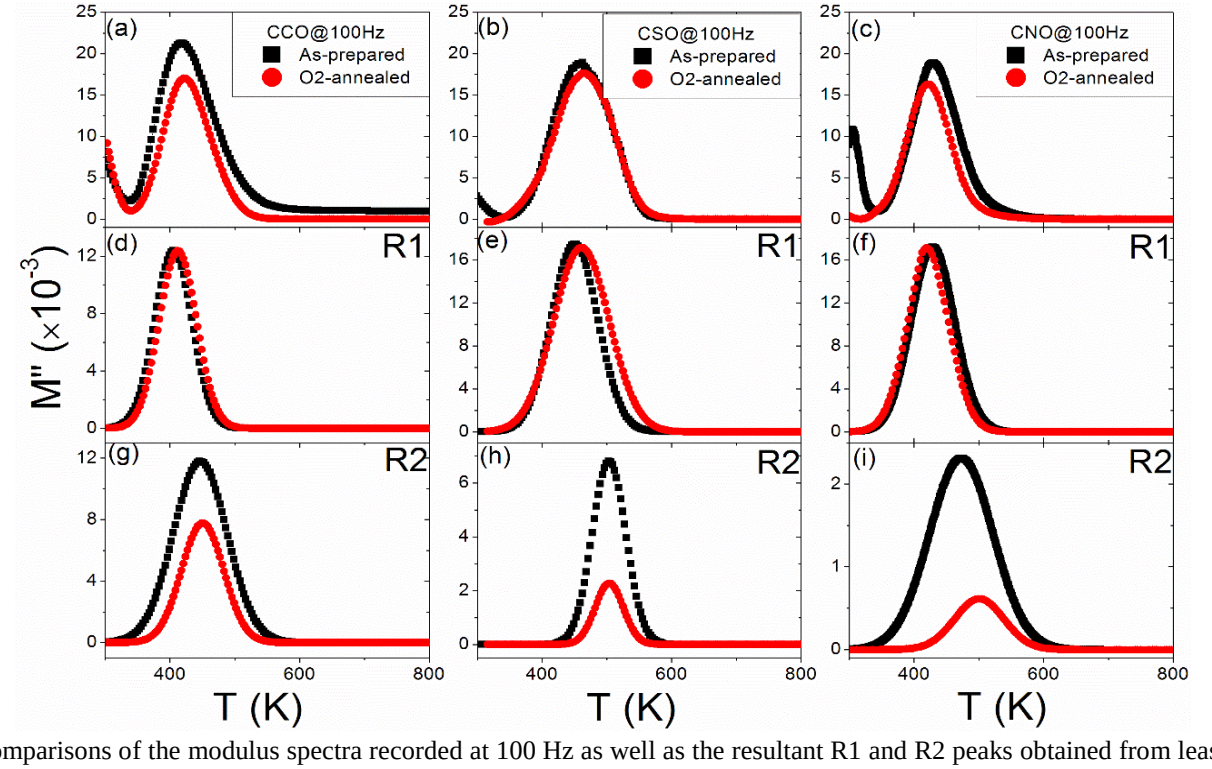

Fig. 8 Comparisons of the modulus spectra recorded at 100 Hz as well as the resultant R1 and R2 peaks obtained from least-square fittings between the as-prepared and O_2-annealed cases for CCO (a,d,g), CSO (b,e,h), and CNO (c,f,i).

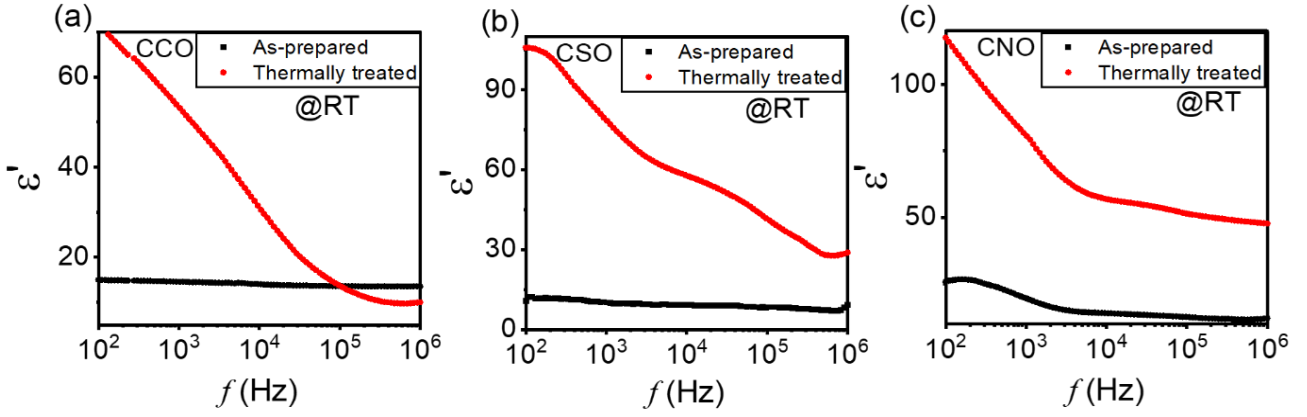

Fig. 9 Frequency dependence of the as-prepared and thermally treated samples for CCO, CSO, and CNO recorded at room temperature.

To verify this point, the as-prepared CCO, CSO, and CNO pellets were subjected to annealing treatments in O_2 at 800 ℃ for 2 h. After thermal treatment, the dielectric properties were measured as a function of temperature. Fig. 8(a), 8(b), and 8(c) show the comparison of the $M''(T)$ curves recorded at 100 Hz between the as-prepared and O_2-annealed cases for CCO, CSO, and CNO, respectively. The peak comparisons of R1 and R2 detached in terms of least-squares fittings are present in Fig. 8(d)-(f) and (g)-(i), respectively. It is seen that peak R2 is depressed by the O_2 annealing treatment, further confirming that this peak is related to V_Os. However, peak R1 is independent of the treatment. This fact evidences that R_1 has nothing to do with the V_Os, and therefore, the V_O-dopant defect associates are unlikely the origin of R1.

As mentioned earlier, the origin of R1 had been assigned to the vacancy-dopant defect pairs, but if this is the case, then R1 should be non-existent in pure ceria as well.[17] In addition, this relaxation should have been depressed under annealing treatments. Hence, there is a need to understand the underlying phenomenon of relaxation R1. For this purpose, the samples were subjected to annealing treatments at 900 ℃ for 2h and were air-quenched to measure the frequency-dependent dielectric properties at room temperature immediately. The annealing treatment and air-quenching ensured the complete removal of adsorbed water molecules onto the samples' surface. The results of as-prepared and thermally treated samples are shown in Fig. 9. It can be seen that the dielectric permittivity of the thermally treated samples has increased as compared to the as-prepared ones. Therein, the low-temperature relaxation R1 was ascribed to be a Maxwell-Wagner relaxation caused by humidity sensitivity. To clarify this, we conducted XPS and humidity response measurements. Fig. 10 shows the capacitance curves as a function of time for the samples recorded by changing their environment RH level between 11% and 96%. The samples' humidity response exhibits two prominent features: (1) the capacitance curves show significant change as RH level changes, further demonstrating the humidity sensitive nature of the samples. (2) the capacitance variation rapidly decreases with increasing the measurement frequency signalling the classic Maxwell-Wagner behaviour.[24] Based on this feature, it follows that R1 is a Maxwell-Wagner relaxation caused by humidity sensitivity. As the samples have a pretty porous structure that promotes the surface to adsorb water molecules. These water molecules form a layer on the surface of the sample and can interact with the oxygen vacancies present there; as evident

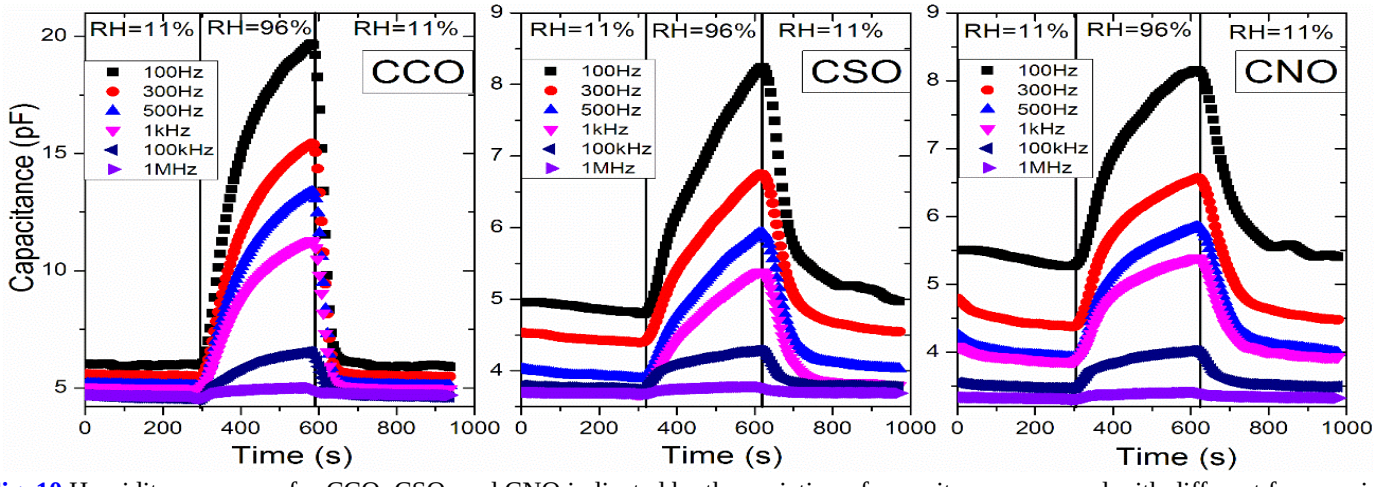

Fig. 10 Humidity responses for CCO, CSO, and CNO indicated by the variation of capacitance measured with different frequencies by switching the RH level between 11% and 95%.

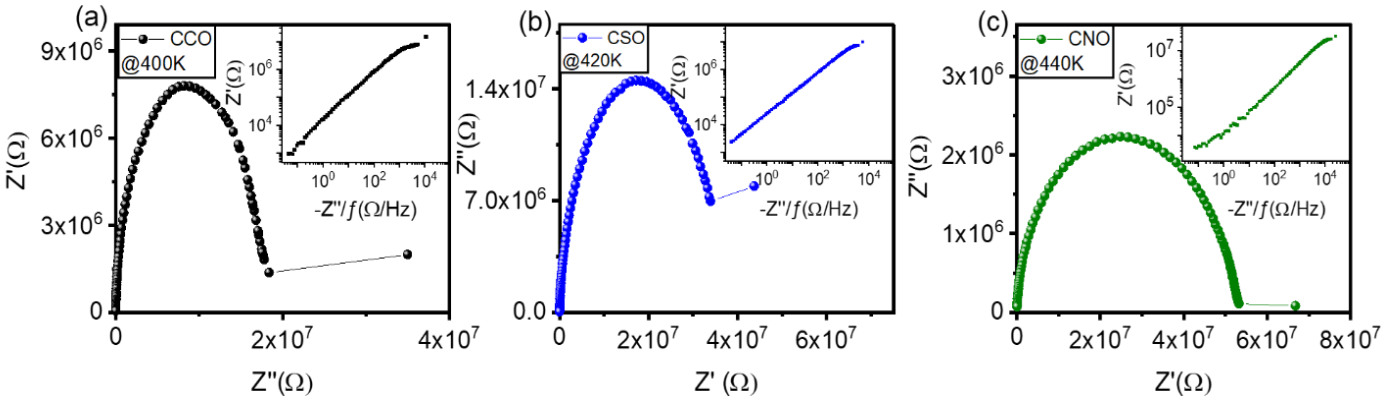

Fig. 11 Nyquist plots for (a) CCO, (b) CSO, and (c) CNO recorded at 400K, 420K and 440K, respectively. The corresponding Z′ versus Z″/f plots are shown in insets.

by the XPS analysis; and can generate positively charged hydroxyl ion defects ($OH_o^{\cdot}$). These hydroxyl ion defects combine with Ce ions to form $OH_o^{\cdot}$-Ce dipoles in the samples. Under the action of external fields, these dipoles can easily re-orientate and generate dipolar relaxation R_1. The reduction of permittivity in thermally treated and air-quenched samples supports the above result.[25-28]

Fig. 11 shows the Cole-Cole plots of CCO, CSO and CNO at 400, 420 and 440K temperature, respectively, as it can tell the contribution of bulk and interface towards dielectric properties. However, it is difficult to differentiate the bulk contribution from the interfacial effects solely from Cole-Cole plots. To get a better understanding, Z′ versus Z″/f was plotted as shown in the insets of Fig. 11. This is a powerful tool to decipher the interfacial effect information. This plot can effectively represent the effect of contacts, grain boundaries and bulk in a low to high-frequency spectrum with just the help of three straight lines. It can be seen in Fig. 11 that the graphs at the low-frequency region deviate from the straight lines. This horizontal deviation indicates the dominating effect of interfacial contribution because of the adsorbed humidity layer onto the sample's surface, giving rise to R1. This effect can also be realized in the samples' Cole-Cole plots, where two semi-circular arcs are seen with a little tail at lower frequency.[29-30]

4. Conclusion

A comprehensive study of the dielectric properties of $Ce_{1-x}CaxO_{2-\delta}$, $Ce_{1-x}Sm_xO_{2-\delta}$, and $Ce_{1-x}Nd_xO_{2-\delta}$ with x=0.1, 0.2, and 0.3, respectively, was performed. All three materials show two thermally activated relaxations labelled as R1 and R2. The O_2-annealing treatments prove that the high-temperature relaxation R2 results from the hopping motion of oxygen vacancies as it was depressed under the annealing treatment. While the low-temperature relaxation R1 was unaffected by the annealing treatment. A comparison of the dielectric properties of the as-prepared and thermally treated samples and humidity sensitivity measurements showed that R1 is a Maxwell-Wagner relaxation caused by $OH_o^{\cdot}$-Ce dipoles due to adsorbed humidity. The Nyquist plots of CCO, CSO and CNO at 400, 420 and 440K also verified this finding.

Acknowledgements

The authors acknowledge financial support from the National Natural Science Foundation of China (Grant no. 51872001 and 51502001). This work was supported in part by the Open Research Fund Program of the State Key Laboratory of Low-Dimensional Quantum Physics (Grant no. KF201802).

Supporting information

Applicable.

Conflict of interest

There are no conflicts to declare.

References

[1] T. H. Santos, J. P. F. Grilo, F. J. A. Loureiro, D. P. Fagg, F. C. Fonseca, D. A. Macedo, *Ceram. Int.*, 2018, **44**, 2745–2751. doi: 10.1016/j.ceramint.2017.11.009.

[2] A.-K. Elger, J. Baranyai, K. Hofmann, C. Hess, Direct Operando Spectroscopic Observation of Oxygen Vacancies in Working Ceria-Based Gas Sensors, *ACS Sensors*, 2019. doi: 10.1021/acssensors.9b00521.

[3] F. Zhou, X. Song, X. Zhou, J. Gao, J. Bao, Z. Tian, S. An, *Ceram. Int.*, 2019, **45**, 12060–12065.doi: 10.1016/j.ceramint.2019.03.102.

[4] S.I. Ahmad, T. Mohammed, A. Bahafi, M.B. Suresh, *Appl. Nanosci.*, 2017, **7**, 243–252. doi: 10.1007/s13204-017-0567-x.

[5] K. C. Anjaneya, G.P. Nayaka, J. Manjanna, G. Govindaraj, K.N. Ganesha, *J. Alloy Compd.*, 2013, **578**, 53–59. doi: 10.1016/j.jallcom.2013.05.010.

[6] K. Eguchi, T. Setoguchi, T. Inoue, H. Arai, *Solid State Ionics.*, 1992, **52**, 165–172. doi: 10.1016/0167-2738(92)90102-U.

[7] B. Ji, C. Tian, C. Wang, T. Wu, J. Xie, M. Li, *J. Power Sources.*, 2015, **278,** 420–429, doi: 10.1016/j.jpowsour.2014.12.073.

[8] K.C. Anjaneya, G. P. Nayaka, J. Manjanna, V. M. A. Kumar, G. Govindaraj, K. N. Ganesha, *J. Alloy Compd.*, 2014, **598**, 33–40, doi: 10.1016/j.jallcom.2014.01.242.

[9] R. Ahmed, S. ur Rehman, R. Si, C. Wang, *Phys. Status Solidi B.*, 2021, **258**, 2000342, doi:10.1002/pssb.202000342.
[10] R. Ahmed, J. Wang, R.J. Si, S. ur Rehman, T. Li, H. Bi, Y. Yu, Q.J. Li, Y.D. Li, S.G. Huang, *J. Eur. Ceram. Soc.*, 2021, **41**, 2625–2632, doi: 10.1016/j.jeurceramsoc.2020.11.034.
[11] R. Ahmed, R. Si, S. ur Rehman, Y. Yu, Q. Li, C. Wang, *Results Phys.*, 2021, **20**, 103623, doi: 10.1016/j.rinp.2020.103623.
[12] R. Ahmed, R. Si, S. ur Rehman, Y. Yu, Q. Li, C. Wang, *Phys. B Condens. Matter.*, 2021, **603**, 412704, doi: 10.1016/j.physb.2020.412704.
[13] M. Burbano, S.T. Norberg, S. Hull, S.G. Eriksson, D. Marrocchelli, P.A. Madden, G.W. Watson, *Chem. Mater.*, 2011, **24**, 222–229, doi: 10.1021/cm2031152.
[14] D. Marrocchelli, P.A. Madden, S.T. Norberg, S. Hull, *Chem. Mater.,* 2011, **23**, 1365–1373, doi: 10.1021/cm102809t.
[15] S. ur Rehman, H. Bi, Electrodes for Flexible Integrated Supercapacitors, Flex. Supercapacitor Nanoarchitectonics. 2021, 1–26. doi: 10.1002/9781119711469.ch1.
[16] P. Sarkar, P.S. Nicholson, *J. Phys. Chem. Solids.*, 1989, **50**, 197–206, doi: 10.1016/0022-3697(89)90418-6.
[17] J.S. Kim, *J. Phys. Soc. Japan.* 2001, **70**, 3129–3133, doi: 10.1143/jpsj.70.3129.
[18] H. Yamamura, S. Takeda, K. Kakinuma, *Solid State Ionics.*, 2007, **178**, 1059–1064, doi: 10.1016/j.ssi.2007.05.010.
[19] H. Yamamura, S. Takeda, K. Kakinuma, *J. Ceram. Soc. Japan.*, 2007, **115**, 471–474, doi: 10.2109/jcersj2.115.471.
[20] A. Hassan, M.A. Aslam, M. Bilal, M.S. Khan, S. ur Rehman, K. Ma, J. Wang, Z. Sheng, *Ceram. Int.* 2021, doi: 10.1016/j.ceramint.2021.04.014.
[21] C. Artini, M. Pani, M. M. Carnasciali, M. T. Buscaglia, J.R. Plaisier, G. A. Costa, *Inorg. Chem.*, 2015, **54**, 4126–4137, doi: 10.1021/acs.inorgchem.5b00395.
[22] S. ur Rehman, M. Sun, M. Xu, J. Liu, R. Ahmed, M. Adnan Aslam, R. Ali Ahmad, H. Bi, *J. Colloid Interf. Sci.*, 2020, **574**, 87-96, doi: 10.1016/j.jcis.2020.04.053.
[23] S. ur Rehman, R. Ahmed, J. Liu, J. Wang, M. Sun, Z. Fang, M.A. Aslam, P.C. Morais, C. Wang, H. Bi, *Part. Syst. Charact.*, 2019, **36**, 1900047, doi: 10.1002/ppsc.201900047.
[24] Y. Wang, Y. Liu, C. Wang, H. Liu, J. Zhang, J. Lin, J. Fan, T. Ding, J.E. Ryu, Z. Guo, *Eng. Sci.,* 2020, **9,** 50–59. doi: 10.30919/es8d903.
[25] S. ur Rehman, J. Wang, Q. Luo, M. Sun, L. Jiang, Q. Han, J. Liu, H. Bi, *Chem. Eng. J.*, 2019, **373**, 122–130. doi: 10.1016/j.cej.2019.05.040.
[26] R. Nie, Q. Wang, P. Sun, R. Wang, Q. Yuan, X. Wang, *Eng. Sci.,* 2019, **6**, 22–29, doi: 10.30919/es8d668.
[27] S. ur Rehman, R. Ahmed, K. Ma, S. Xu, T. Tao, M.A. Aslam, M. Amir, J. Wang, *Eng. Sci.*, 2020, **13**, 71–78, doi: 10.30919/es8d1263.
[28] Sajid ur Rehman, J. Liu, Z. Fang, J. Wang, R. Ahmed, C. Wang, H. Bi, *ACS Appl. Nano Mater.*, 2019, **2**, 4451–4461, doi: 10.1021/acsanm.9b00841.
[29] W. Uddin, S. ur Rehman, M.A. Aslam, S. ur Rehman, M. Wu, M. Zhu, *Mater. Res. Bull.*, 2020, **130**, 110943, doi: 10.1016/j.materresbull.2020.110943.
[30] H. Huang, L. Han, Y. Wang, Z. Yang, F. Zhu, M. Xu, *Eng. Sci.*, 2019, **9**, 60–67, doi: 10.30919/es8d812.
[31]M.C. Biesinger, B.P. Payne, A.P. Grosvenor, L.W.M. Lau, A.R. Gerson, R.S.C. Smart, *Appl. Surf. Sci.*, 2011, **257**, 2717–2730, doi: 10.1016/j.apsusc.2010.10.051.
[32] R. Ahmed, S. T. Wang, J. Sun, J. Wang, T. Y. Li, Y. Yu, Q. J. Li, C. C. Wang, *Ceram. Int.*, 2019, **45**, 13484–13487, doi: 10.1016/j.ceramint.2019.04.051.

Author information

Rida Ahmed *received her PhD degree in Materials Physics from Anhui University, Hefei, P. R. China. Her research is focused on dielectric materials and energy storage devices.*

Shuting Wang *received her Master's degree in Materials Physics from Anhui University, Hefei, P. R. China. Her research is focused on dielectric materials and energy storage devices*

Sajid ur Rehman *received his PhD degree in Polymer Chemistry and Physics from Anhui University, Hefei, China. Currently, he is on Post-doctoral position at High Magnetic Field Laboratory, Hefei Institute of Physical Sciences, Chinese Academy of Sciences, Hefei, China. His research focus is on biomaterials, energy storage devices and microwave absorption properties.*

Sun Jie *received his Master's degree in Materials Physics from Anhui University, Hefei, P. R. China. His research is focused on dielectric materials and energy storage devices.*

Wang Jin *received his Master's degree in Materials Physics from Anhui University, Hefei, P. R. China. His research is focused on dielectric materials and energy storage devices.*

Si Renjun *doing his Master's degree in Materials Physics from Anhui University, Hefei, P. R. China. His research is focused on dielectric materials and humidity sensors.*

An Kang Zhu *is doing his Ph.D. degree in Materials Physics from Anhui University, Hefei, P. R. China. His research is focused on solid oxide fuel cells.*

Chunchang Wang *Currently working in School of Physics and Material Science, Anhui University (AHU). He received his B.S. degree from AHU in 1993, M.S. degree from Institute of Solid State Physics, Chinese Academy of Sciences, in 1997, and PH. D. degree from Tsinghua University in 2004. Before joining AHU, he was a Researcher Fellow first at National Institute of Advanced Industrial Science and Technology, Japan, then at University of Wollongong, Australia. His research interests include dielectric physics and the applications of dielectric materials in the fields of energy storage, sensors, and photocatalysis.*